Contribution from the Laboratoire de Synthèse et d'Electrosynthèse Organométallique associé au CNRS (UA 33), Faculté des Sciences "Gabriel", 21100 Dijon, France, Laboratoire de Minéralogie et Cristallographie associé au CNRS (UA 809), Faculte des Sciences, Centre de 2eme Cycle, 54506 Vandoeuvre les Nancy, France, and Department of Chemistry, University of Houston, Houston, Texas 77004

Metalloporphyrins with Metal–Metal Bonds. Synthesis and Characterization of (P)InMn(CO)$_5$, (P)InCo(CO)$_4$, and (P)InM(CO)$_3$Cp Where M = Cr, Mo, and W. Molecular Stereochemistry of [(2,3,7,8,12,13,17,18-Octaethylporphyrinato)indium(III)]pentacarbonylmanganese

R. Guilard,*[1a] P. Mitaine,[1a,c] C. Moïse,[1a] C. Lecomte,[1b] A. Boukhris,[1b] C. Swistak,[1c] A. Tabard,[1a,c] D. Lacombe,[1c] J.-L. Cornillon,[1c] and K. M. Kadish*[1c]

Received December 11, 1986

The synthesis and physicochemical characterization of 10 metal–metal-σ-bonded indium porphyrins were investigated in nonaqueous media. The ligands σ-bonded to indium tetraphenylporphyrin ((TPP)In) or indium octaethylporphyrin ((OEP)In) were Mn(CO)$_5$, Co(CO)$_4$, W(CO)$_3$Cp, Mo(CO)$_3$Cp, and Cr(CO)$_3$Cp. Each neutral complex was characterized by ^{1}H NMR, IR, and UV–visible spectroscopy. On the basis of these data, the presence of a single metal–metal covalent bond was suggested, and this was confirmed by a room-temperature single-crystal X-ray diffraction study. (OEP)InMn(CO)$_5$ crystallizes in the triclinic system, space group $P\bar{1}$. Its lattice constants are as follows: a = 12.415 (3) Å, b = 13.485 (2) Å, c = 15.083 (3) Å, α = 61.99 (2)°, β = 69.69 (2)°, and γ = 69.75 (2)° with Z = 2 (D_{expt} = 1.44 g·cm^{-3}), $R(F)$ = 0.041, and $R_w(F)$ = 0.048 for 7346 unique reflections. The In–Mn bond length is 2.705 (1) Å, and the indium atom lies 0.744 (1) Å from the plane of the four porphyrin nitrogens. The average Mn–CO equatorial distance (1.839 (4) Å) is longer than the axial one (1.809 (6) Å). The electrochemistry of each σ-bonded complex was carried out in methylene chloride containing 0.1 M (TBA)PF$_6$. Each metalloporphyrin could be electrooxidized, but the bimetallic complex underwent a rapid cleavage of the metal–metal bond after the first one-electron abstraction. The complexes could also be reversibly reduced by one or two electrons, but a cleavage of the metal–metal bond invariably occurred, leading to formation of (P)In$^\bullet$ and [ML]$^-$ entities. Some of the reduced compounds were stable for short times that depended upon the specific axial ligand. In these cases a characterization of the reduced species was carried out. Finally, comparisons were made between the reactivities and physicochemical properties of the investigated complexes and other alkyl or aryl σ-bonded indium porphyrins that have been described in the literature.

Introduction

The synthesis and characterization of three different classes of metal–metal-bonded metalloporphyrins have appeared in the literature.[2,3] These classes include the following: (i) homobinuclear porphyrins of the type (P)MM(P), where P is one of several different porphyrin rings and M = Ru(II),[4] Os(II),[5] Mo(II),[5,6] Rh(II),[5,7–10] Ir(II);[11] (ii) σ-bonded heteronuclear metalloporphyrin complexes of the type (P)InRh(P),[12] and (P)InM(L);[13] (iii) carbenoid-bonded heteronuclear metalloporphyrins of the type (P)MM′(L).[14–17]

The carbenoid complexes are typified by metalloporphyrins of tin and germanium that are coordinated with Fe(CO)$_4$, Mn(CO)$_4$HgMn(CO)$_5$, or Co(CO)$_3$HgCo(CO)$_4$ units.[14–17] These donor–acceptor complexes have been identified by various physicochemical techniques, and X-ray structures of (OEP)SnFe(CO)$_4$[14] and (TPP)SnMn(CO)$_4$HgMn(CO)$_5$[17] have been published. The former compound has also been examined by IR and Mössbauer spectroscopy and, on the basis of these experiments, Sn(II)–Fe(O) oxidation states have been assigned.[14]

In a preliminary communication,[13] the conversion of (OEP)InCl to (OEP)InM(L) was reported where M(L) was Co(CO)$_4$, Mn(CO)$_5$, Mo(CO)$_3$Cp, or W(CO)$_3$Cp. The metal–metal-bonded OEP derivatives were synthesized by reaction of the metalate anion with (OEP)InCl,[13] and this same technique was more recently utilized for the synthesis of indium tetraphenylporphyrin (TPP) complexes coordinated to Mn(CO)$_5$, Re(CO)$_5$, Co(CO)$_4$, and Co(CO)$_3$P(OPh)$_3$.[17]

This present paper expands the number of reported metal–metal-σ-bonded porphyrins and also presents a complete characterization of these complexes. The investigated compounds were (P)InMn(CO)$_5$, (P)InCo(CO)$_4$, and (P)InM(CO)$_3$Cp, where M = Cr, Mo, W,[18] all of which were electrochemically investigated as to their oxidation and reduction properties. Preliminary electrochemistry has already been reported for reduction of two σ-bonded metalloporphyrins.[19] In addition, we report a novel synthetic method for the preparation of several metal–metal-σ-bonded metalloporphyrins. This method involves reaction of a bimetallic metal carbonyl complex with a σ-bonded alkyl- or arylindium(III) porphyrin. High yields were obtained with this method, which appears to be independent of the nature of the bound alkyl or aryl group. Finally, this paper describes the molecular stereochemistry of [(2,3,7,8,12,13,17,18-octaethylporphyrinato)indium(III)]pentacarbonylmanganese, (OEP)InMn(CO)$_5$.

Experimental Section

Chemicals. Synthesis and handling of the binuclear complexes were carried out under an argon atmosphere. All common solvents were thoroughly dried in an appropriate manner and were distilled under argon prior to use. (TPP)InCl,[20] (OEP)InCl,[20] and the metalate anions[21]

(1) (a) Université de Dijon. (b) Universite de Nancy I. (c) University of Houston.
(2) Guilard, R.; Lecomte, C.; Kadish, K. M. *Struct. Bonding (Berlin)*, in press.
(3) Brothers, P. J.; Collman, J. P. *Acc. Chem. Res.* **1986**, *19*, 209.
(4) Collman, J. P.; Barnes, C. E.; Collins, T. J.; Brothers, P. J. *J. Am. Chem. Soc.* **1981**, *103*, 7030.
(5) Collman, J. P.; Barnes, C. E.; Woo, L. K. *Proc. Natl. Acad. Sci. U.S.A.* **1983**, *80*, 7684.
(6) Collman, J. P.; Woo, L. K. *Proc. Natl. Acad. Sci. U.S.A.* **1984**, *81*, 2592.
(7) Wayland, B. B.; Newman, A. R. *Inorg. Chem.* **1981**, *20*, 3093.
(8) Wayland, B. B.; Newman, A. R. *J. Am. Chem. Soc.* **1979**, *101*, 6472.
(9) Setsune, J. I.; Yoshida, Z. I.; Ogoshi, H. *J. Chem. Soc., Perkin Trans. 1* **1982**, 983.
(10) Ogoshi, H.; Setsune, J.; Yoshida, Z. I. *J. Am. Chem. Soc.* **1977**, *99*, 3869.
(11) Del Rossi, K. J.; Wayland, B. B. *J. Chem. Soc., Chem. Commun.* **1986**, 1653.
(12) Jones, N. L.; Carroll, P. J.; Wayland, B. B. *Organometallics* **1986**, *5*, 33.
(13) Cocolios, P.; Moïse, C.; Guilard, R. *J. Organomet. Chem.* **1982**, *228*, C43.
(14) Barbe, J.-M.; Guilard, R.; Lecomte, C.; Gerardin, R. *Polyhedron* **1984**, *3*, 889.
(15) Kadish, K. M.; Boisselier-Cocolios, B.; Swistak, C.; Barbe, J.-M.; Guilard, R. *Inorg. Chem.* **1986**, *25*, 121.
(16) Kadish, K. M.; Swistak, C.; Boisselier-Cocolios, B.; Barbe, J.-M.; Guilard, R. *Inorg. Chem.* **1986**, *25*, 4336.
(17) Onaka, S.; Kondo, Y.; Yamashita, M.; Tatematsu, Y.; Kato, Y.; Goto, M.; Ito, T. *Inorg. Chem.* **1985**, *24*, 1070.
(18) The investigated porphyrins, P, were OEP^{2-} and TPP^{2-}, which represent the dianions of octaethylporphyrin and tetraphenylporphyrin, respectively.
(19) Cocolios, P.; Chang, D.; Vittori, O.; Guilard, R.; Moïse, C.; Kadish, K. M. *J. Am. Chem. Soc.* **1984**, *106*, 5724.
(20) Buchler, J. M.; Eikelman, G.; Puppe, L.; Rohbock, K.; Schneehage, H. H.; Weck, D. *Justus Liebigs Ann. Chem.* **1971**, *745*, 135.
(21) Piper, T. S.; Wilkinson, G. *J. Inorg. Nucl. Chem.* **1956**, *3*, 104.

0020-1669/87/1326-2467$01.50/0

Table I. Percent Yield and Analytical Data for (P)InM(L) Complexes

complexes, (P)InM(L)	mol formula	recrystn solvent[a]	yield, % method A	method B	method C	lit.[b]	anal. data[c] % C	% H	% N	% In	% M
(TPP)InMn(CO)$_5$	$C_{49}H_{28}N_4InMnO_5$	A	69			44	62.1 (63.80)	2.9 (3.06)	6.0 (6.07)	11.2 (12.45)	5.6 (5.96)
(TPP)InCo(CO)$_4$	$C_{48}H_{28}N_4InCoO_4$	A/B (4/1)	20	78	85	72	63.8 (61.16)	3.3 (3.14)	5.9 (6.24)	12.3 (12.78)	5.8 (6.56)
(TPP)InCr(CO)$_3$Cp	$C_{52}H_{33}N_4InCrO_3$	A/B (4/1)	30				67.9 (67.25)	3.8 (3.58)	6.1 (6.03)	13.2 (12.36)	3.5 (5.60)
(TPP)InMo(CO)$_3$Cp	$C_{52}H_{33}N_4InMoO_3$	A/B (4/1)	69	22			64.2 (64.22)	3.4 (3.42)	5.7 (5.76)	10.4 (11.81)	10.4 (9.86)
(TPP)InW(CO)$_3$Cp	$C_{52}H_{33}N_4InWO_3$	A/B (4/1)	70				59.4 (58.90)	3.1 (3.14)	4.8 (5.28)	9.7 (10.83)	20.5 (17.33)
(OEP)InMn(CO)$_5$	$C_{41}H_{44}N_4InMnO_5$	A/B (1/4)	69				59.1 (58.43)	5.4 (5.26)	6.7 (6.65)	13.9 (13.63)	5.6 (6.52)
(OEP)InCo(CO)$_4$	$C_{40}H_{44}N_4InCoO_4$	A/B (1/4)	20	76	81		58.7 (58.69)	5.4 (5.42)	6.9 (6.84)	13.0 (14.03)	7.1 (7.20)
(OEP)InCr(CO)$_3$Cp	$C_{44}H_{49}N_4InCrO_3$	A/B (1/4)	30				56.3 (62.27)	5.5 (5.82)	6.1 (6.60)	13.3 (13.53)	4.1 (6.13)
(OEP)InMo(CO)$_3$Cp	$C_{44}H_{49}N_4InMoO_3$	A/B (1/4)	70	29			58.2 (59.20)	5.5 (5.53)	6.1 (6.28)	14.3 (12.86)	11.2 (10.75)
(OEP)InW(CO)$_3$Cp	$C_{44}H_{49}N_4InWO_3$	A/B (1/4)	70				54.0 (53.90)	4.8 (5.04)	5.7 (5.71)	11.7 (11.71)	18.9 (18.75)

[a] Legend: A = toluene; B = heptane. [b] Reference 17. [c] Calculated values in parentheses.

$[Mn(CO)_5]^-$, $[Co(CO)_4]^-$, $[Cr(CO)_3Cp]^-$, $[Mo(CO)_3Cp]^-$, and $[W(CO)_3Cp]^-$ were synthesized by literature procedures. Reagent grade methylene chloride (CH_2Cl_2, Fisher) and benzonitrile (PhCN, Aldrich) were used for electrochemical studies and were distilled from P_2O_5 before use. Tetrabutylammonium hexafluorophosphate ((TBA)PF_6) was purchased from Alfa and was recrystallized from ethyl acetate/hexane mixtures prior to use.

Syntheses. Three general procedures were utilized for preparation of the dinuclear complexes. These are as follows:

Method A. Solid metalate ion (0.38 mmol) was added in the dark to (P)InCl (0.33 mmol) in 150 mL of tetrahydrofuran. The reaction was monitored by IR spectroscopy in the CO stretching region. After about 12 h THF was evaporated at room temperature and the resulting solid was chromatographed in the dark over a basic alumina column using a benzene/heptane mixture as eluent under an argon atmosphere. The crude product was recrystallized from toluene/heptane. The yields for this method are given in Table I and varied between 20 and 70% depending upon the specific metalate anion.

Method B: Synthesis of (P)InCo(CO)$_4$ and (P)InMo(CO)$_3$Cp. Dimeric $Co_2(CO)_8$ or $[Mo(CO)_3Cp]_2$ (0.38 mmol) was mixed with (P)In(CH_3) (0.33 mmol) in 150 mL of THF. The solution was irradiated and the reaction monitored by taking IR spectra in the carbonyl stretching region. The reaction was generally complete after 2 h. Purification and recrystallization of the final product were similar to that described in method A. The yields by this method are given in Table I.

Method C: Synthesis of (P)InCo(CO)$_4$. Dimeric $Co_2(CO)_8$ (0.38 mmol) was mixed with (P)InCl (0.33 mmol) in 150 mL of THF. The reaction was complete after 1 h as shown by IR spectroscopy. Again, the purification and recrystallization were similar to that of method A. The product yields by this method are given in Table I and were over 80%.

Physicochemical Measurements. Elemental analyses were performed by the "Service de Microanalyses du CNRS". Mass spectra were recorded in the electron-impact mode with the Finnigan 3300 spectrometer (ionizing energy 30–70 eV, ionizing current 0.4 mA, source temperature 250–400 °C). ^1H NMR spectra were recorded at 400 MHz on a Bruker WM 400 spectrometer of the Cerema ("Centre de Resonance Magnetique" of the University of Dijon). Spectra were measured from 5-mg solutions of the complex in C_6D_6 with tetramethylsilane as an internal reference. ESR spectra were recorded at 115 K on an IBM Model ER 100 D spectrometer equipped with a microwave ER-040-X bridge and an ER 080 power supply. The g values were measured with respect to diphenylpicrylhydrazyl (g = 2.0036 ± 0.0003). Infrared spectra were obtained on a Perkin-Elmer 580 B apparatus. Samples were prepared as either a 1% dispersion in CsI pellets or in THF solutions. Electronic absorption spectra were recorded on a Perkin-Elmer 559 spectrophotometer, an IBM Model 9430 spectrophotometer, or a Tracor Northern 1710 holographic optical spectrophotometer–multichannel analyzer. For the photochemical reactions, an OSRAM HQI-T400W/DV mercury lamp was used (power 360 W, 28 000 lm in the visible spectral range).

Cyclic voltammetric measurements were obtained with the use of a three-electrode system. The working electrode was a platinum button, and the counter electrode was a platinum wire. A saturated calomel electrode (SCE) was used as the reference electrode and was separated from the bulk of the solution by a fritted-glass bridge. A BAS 100 electrochemical analyzer connected to a Houston Instruments HIPLOT DMP 40 plotter was used to measure the current–voltage curves.

Controlled-potential electrolyses were performed with an EG&G Model 173 potentiostat or a BAS electrochemical analyzer. Both the reference electrode and the platinum-wire counter electrode were separated from the bulk of the solution by means of a fritted-glass bridge. Thin-layer spectroelectrochemical measurements were performed with an IBM EC 225 voltammetric analyzer coupled with a Tracor Northern 1710 holographic optical spectrometer–multichannel analyzer to give time-resolved spectral data. The utilized optically transparent platinum thin-layer electrode (OTTLE) has been described in a previous publication.[22]

Crystal and Molecular Structure Determination. A suitable crystal of (OEP)InMn(CO)$_5$ was obtained from recrystallization of the complex

Table II. Experimental Conditions

formula	$C_{41}H_{44}N_4InMnO_5$
fw	842.6
space group	triclinic, $P\bar{1}$
cryst size, mm^3	0.32 × 0.24 × 0.20
cryst color	black
lattice params	
a, b, c, Å	12.415 (3), 13.485 (2), 15.083 (3)
α, β, γ, deg	61.99 (2), 69.69 (2), 69.75 (2)
V, Z; ρ_{calcd}, g·cm^{-3}	1937.3 (4); 2; 1.44
μ(Cu Kα), cm^{-1}	75.79
diffractometer	Enraf-Nonius CAD4F (room temp)
radiation	Cu Kα (graphite monochromatized)
scan type; (sin θ)/λ max, Å^{-1}	ω–2θ; 0.63
scan range, deg; scan speed deg·min^{-1}	1 + 0.35 tan θ; 0.25 < v < 0.5
aperture, mm	3.2 + tan θ
hkl limits	$-15 < h < 15$; $-16 < k < 16$; $0 < l < 18$
no. of reflcns measd	8296
no. of reflcns used (N)	7346 ($I > 3\sigma(I)$)
no. of params (N_p)	468
N/N_p	15.7
program used	SDP,[23] SHELX[24]
$R(F)$	0.041
$R_w(F)$	0.048
w	$1/[\sigma^2(F) + 0.0078F^2]$
Δ/σ_{max}	0.5 (for Z of C(35))
GOF	0.81
max residual density, e/Å^3	1.0 (on In)

(22) Lin, X. Q.; Kadish, K. M. *Anal. Chem.* **1985**, *57*, 1498.

Table III. Fractional Coordinates, Standard Deviations, and Equivalent Temperature Factors (Å²) of [(2,3,7,8,12,13,17,18-Octaethylporphyrinato)indium(III)]pentacarbonylmanganese

atom	*x*	*y*	*z*	*B*
In	0.15464 (2)	0.17550 (2)	0.29003 (2)	2.624 (7)
Mn	0.32822 (5)	0.30629 (5)	0.20687 (5)	3.68 (2)
O1	0.1146 (4)	0.4743 (3)	0.2811 (4)	8.1 (2)
O2	0.3332 (4)	0.1965 (4)	0.4278 (3)	8.5 (2)
O3	0.5070 (3)	0.1119 (4)	0.1495 (4)	7.9 (2)
O4	0.2777 (4)	0.3897 (4)	0.0075 (3)	5.7 (1)
O5	0.5182 (4)	0.4483 (4)	0.1139 (4)	9.6 (2)
N1	−0.0317 (3)	0.2745 (2)	0.3344 (2)	3.23 (8)
N2	0.1115 (3)	0.1868 (2)	0.1601 (2)	3.22 (8)
N3	0.2478 (3)	0.0041 (2)	0.2906 (2)	3.20 (8)
N4	0.1021 (3)	0.0907 (2)	0.4660 (2)	3.05 (8)
CO1	0.1953 (5)	0.4090 (4)	0.2532 (4)	5.4 (1)
CO2	0.3318 (4)	0.2358 (4)	0.3436 (4)	5.4 (1)
CO3	0.4374 (4)	0.1844 (4)	0.1729 (4)	5.1 (1)
CO4	0.2966 (4)	0.3580 (4)	0.0833 (4)	4.8 (1)
CO5	0.4451 (5)	0.3934 (4)	0.1498 (4)	5.8 (2)
C1	−0.0891 (3)	0.2997 (3)	0.4254 (3)	3.16 (9)
C2	−0.1874 (3)	0.3965 (3)	0.4107 (3)	3.5 (1)
C3	−0.1852 (3)	0.4281 (3)	0.3112 (3)	3.4 (1)
C4	−0.0867 (3)	0.3494 (3)	0.2623 (3)	3.19 (9)
C5	−0.0557 (3)	0.3500 (3)	0.1606 (3)	3.5 (1)
C6	0.0326 (3)	0.2733 (3)	0.1151 (3)	3.22 (9)
C7	0.0558 (8)	0.2700 (3)	0.0127 (3)	3.33 (9)
C8	0.1529 (3)	0.1818 (3)	−0.0041 (3)	3.5 (1)
C9	0.1854 (3)	0.1319 (3)	0.0892 (3)	3.16 (9)
C10	0.2764 (3)	0.0358 (3)	0.1081 (3)	3.4 (1)
C11	0.3024 (3)	−0.0252 (3)	0.2013 (3)	3.27 (9)
C12	0.3905 (3)	−0.1293 (3)	0.2210 (3)	3.6 (1)
C13	0.3883 (3)	−0.1584 (3)	0.3214 (3)	3.6 (1)
C14	0.2968 (3)	−0.0749 (3)	0.3651 (3)	3.12 (9)
C15	0.2620 (3)	−0.0783 (3)	0.4688 (3)	3.7 (1)
C16	0.1720 (3)	−0.0020 (3)	0.5152 (3)	2.97 (9)
C17	0.1379 (3)	−0.0095 (3)	0.6246 (3)	3.19 (9)
C18	0.0473 (3)	0.0805 (3)	0.6380 (3)	3.14 (9)
C19	0.0247 (3)	0.1428 (3)	0.5382 (3)	2.98 (9)
C20	−0.0628 (3)	0.2404 (3)	0.5183 (3)	3.24 (9)
C25	−0.2665 (4)	0.4535 (4)	0.4923 (4)	4.6 (1)
C26	−0.1987 (6)	0.5281 (5)	0.4920 (6)	8.2 (3)
C27	−0.2723 (4)	0.5180 (3)	0.2586 (4)	4.6 (1)
C28	−0.3834 (5)	0.4711 (5)	0.2843 (5)	6.9 (2)
C29	−0.0199 (4)	0.3445 (3)	−0.0572 (3)	4.2 (1)
C30	−0.1411 (5)	0.3031 (5)	−0.0135 (4)	6.1 (2)
C31	0.2111 (4)	0.1436 (4)	−0.0966 (3)	4.4 (2)
C32	0.1669 (5)	0.0389 (5)	−0.0721 (4)	6.6 (2)
C33	0.4636 (3)	−0.1900 (3)	0.1440 (3)	4.3 (1)
C34	0.3877 (4)	−0.2618 (4)	0.1486 (4)	5.7 (2)
C35	0.4671 (4)	−0.2534 (3)	0.3801 (4)	4.6 (1)
C36	0.5628 (4)	−0.2119 (5)	0.3847 (4)	5.6 (2)
C37	0.1968 (4)	−0.0979 (3)	0.7017 (3)	4.3 (1)
C38	0.3227 (5)	−0.0759 (5)	0.6755 (5)	6.6 (2)
C39	−0.0172 (4)	0.1156 (4)	0.7335 (3)	4.0 (1)
C40	0.0303 (5)	0.2157 (5)	0.7158 (4)	6.7 (2)

in a solution of toluene/heptane (1:4). Oscillation and Weissenberg photographs along the needle axis did not reveal any symmetry. The experimental conditions are given in Table II. Data reduction was made by using the SDP package,[23] and no decay was observed. No adsorption correction was made. Fractional coordinates of the indium and manganese atoms were calculated from the Patterson map. Subsequent sets of Fourier and difference Fourier syntheses in the $P\bar{1}$ space group then revealed the whole crystal structure, including the hydrogen atoms. These hydrogen atoms were fixed at the positions found on the $\Delta\rho(r)$ maps with constant isotropic temperature factors ($U(H) = 3.16$ Å²). At the end of the refinement the largest residue was 1.0 e/Å³ on the indium atom. The final agreement factors are given in Table II (SHELX).[24] Atomic scattering factors and anomalous dispersion corrections were taken from ref 24 and 25. Table III gives the fractional coordinates, the standard deviations, and the equivalent temperature factors of the non-hydrogen atoms. Coordinates of the hydrogen atoms, thermal parameters (U_{ij}) of the non-hydrogen atoms, structure factors, bond distances and angles in the porphyrin ligand, and a summary of least-squares planes are given in the supplementary material.

(23) *SDP: Structure Determination Package*; Enraf-Nonius: Delft, The Netherlands, 1977.
(24) Sheldrick, G. M. *Programs for Crystal Structure Determination*; University of Göttingen: Göttingen, West Germany, 1976.
(25) *International Tables for X-ray Crystallography*; Kynoch: Birmingham, U.K., 1974; Vol. IV.

Table IV. Mass Spectral Data of (P)InM(L) Complexes in CH_2Cl_2

porphyrin, P	ligand, M(L)	fragment	*m/e* (%)
TPP	$Mn(CO)_5$	$[(TPP)InMn(CO)_5]^{\cdot+}$	922 (0.7)
		$[(TPP)In]^+$	727 (100.0)
		$[(TPP)Mn]^+$	667 (3.9)
	$Co(CO)_4$	$[(TPP)InCo]^{\cdot+}$	786 (7.9)
		$[(TPP)In]^+$	727 (100.0)
	$Cr(CO)_3Cp$	$[(TPP)InCr]^{\cdot+}$	779 (0.6)
		$[(TPP)In]^+$	727 (100.0)
		$[(TPP)Cr]^+$	664 (1.3)
	$Mo(CO)_3Cp$	$[(TPP)MoCp]^+$	773 (1.5)
		$[(TPP)In]^+$	727 (100.0)
	$W(CO)_3Cp$	$[(TPP)WCp]^+$	861 (1.4)
		$[(TPP)In]^+$	727 (100.0)
OEP	$Mn(CO)_5$	$[(OEP)InMn(CO)_5]^{\cdot+}$	842 (0.8)
		$[(OEP)In]^+$	647 (100.0)
	$Co(CO)_4$	$[(OEP)InCo]^{\cdot+}$	706 (8.8)
		$[(OEP)In]^+$	647 (100.0)
	$Cr(CO)_3Cp$	$[(OEP)InCrH]^+$	698 (0.3)
		$[(OEP)In]^+$	647 (80.0)
		$[(OEP)Cr]^+$	584 (0.8)
	$Mo(CO)_3Cp$	$[(OEP)InMo(CO)_3Cp]^{\cdot+}$	891 (0.3)
		$[(OEP)MoCp]^+$	808 (0.2)
		$[(OEP)In]^+$	647 (100.0)
	$W(CO)_3Cp$	$[(OEP)InW(CO)_3Cp]^{\cdot+}$	980 (1.0)
		$[(OEP)In]^+$	647 (100.0)

Results and Discussion

Synthesis of the (P)InM(L) complexes was accomplished by the three methods described in the Experimental Section. Method A, which involved nucleophilic substitution of the chloride ion on (P)InCl by $[Mn(CO)_5]^-$, $[Co(CO)_4]^-$, $[Cr(CO)_3Cp]^-$, $[Mo(CO)_3Cp]^-$, or $[W(CO)_3Cp]^-$, was the main method of synthesis. Yields by this method are summarized in Table I and suggest the following classification according to the metalate anion reactivity:

$$[Co(CO)_4]^- < [Cr(CO)_3Cp]^- < [Mo(CO)_3Cp]^- \approx [Mn(CO)_5]^- < [W(CO)_3Cp]^-$$

Dessy et al.[26] have reported a similar classification based on the nucleophilic power of the anion.

The reaction yield could be improved by using either of two other synthetic methods. Method B involves a photochemical reaction of the aryl or alkyl σ-bonded porphyrin and dimeric $Co_2(CO)_8$ or $[Mo(CO)_3Cp]_2$. During this reaction the (P)In$^{\bullet}$ ESR radical anion spectrum is observed. Method C was successful only for the synthesis of $(P)InCo(CO)_4$. This synthetic method proceeds via a reaction involving (P)InCl and $Co_2(CO)_8$ in THF. The nature of the solvent is important since the reaction was only observed to occur in THF.

Spectral Measurements. Elemental analysis and mass spectral data of the bimetallic compounds are summarized in Tables I and IV. All of the fragmentation patterns prove the existence of a metal–metal bond in the investigated complexes. The molecular peak is of weak intensity (0.3–1%) and was observed for only a few complexes. Other fragments such as $[(P)M]^+$ or $[(P)MCp]^+$ were also obtained and are due to a transmetalation rearrangement. The parent peak was generally the ionic species $[(P)In]^+$, and this suggests a relatively weak metal–metal bond.

IR spectroscopic studies show that two different types of complexes can be distinguished according to the axial ligand. These are the carbonylmetalate complexes and cyclopentadienyl complexes. For $(P)InM(CO)_3Cp$ compounds in solution, the local symmetry around the axial metal is C_s, suggesting three IR- and Raman-active ν_{CO} modes: 2 A′ + A″ (see Table V).[27–32]

(26) Dessy, R. E.; Pohl, R. L.; King, R. B. *J. Am. Chem. Soc.* **1966**, *88*, 5121.
(27) King, R. B.; Houk, L. W. *Can. J. Chem.* **1969**, *47*, 2959.
(28) Burlitch, J. M.; Petersen, R. B. *J. Organomet. Chem.* **1970**, *24*, C65.

Table V. Solution[a] IR Data and Calculated Force Constants of (P)InM(L) Complexes

porphyrin, P	ligand, M(L)	ν_{CO}, cm^{-1}			k, mdyn/Å		
					k_1	k_2	k[b]
TPP	$Mn(CO)_5$	2078	1974		15.90	15.99	0.25[c]
	$Co(CO)_4$	2070	1999	1970	16.76	16.00	0.33[d]
	$Cr(CO)_3Cp$	1967	1902	1872	14.68	14.85	0.70[e]
	$Mo(CO)_3Cp$	1980	1905	1882	14.88	14.95	0.65[e]
	$W(CO)_3Cp$	1976	1898	1875	14.77	14.87	0.67[e]
OEP	$Mn(CO)_5$	2075	1972		15.86	15.95	0.25[c]
	$Co(CO)_4$	2066	1999	1969	16.78	15.97	0.31[d]
	$Cr(CO)_3Cr$	1963	1897	1872	14.75	14.77	0.62[e]
	$Mo(CO)_3Cp$	1976	1899	1882	14.76	14.93	0.63[e]
	$W(CO)_3Cp$	1973	1892	1877	14.65	14.87	0.65[e]

[a] In THF. [b] Approximation. [c] $k = k_i = k_c = k_c' = k_{t/2}$.[22] [d] $k = k_c = k_t$.[16] [e] $k = k_d = 2k_s$.[18]

Table VI. Solid-State IR Data of (P)InM(L) Complexes[a]

porphyrin, P	ligand, M(L)	ν_{CO}, cm^{-1}				ν_{MCO}, cm^{-1}		ν_{MC}, cm^{-1}		ν_{CH},[b] cm^{-1}		
TPP	$Mn(CO)_5$	2078	1996	1975	1965	670	635	490				
	$Co(CO)_4$	2070	1999	1973	1961	550		480				
	$Cr(CO)_3Cp$	1968	1898	1870		650		580	530	1350		810
	$Mo(CO)_3Cp$	1982	1905	1878		585		520	480	1355		810
	$W(CO)_3Cp$	1979	1899	1871		580				1355		820
OEP	$Mn(CO)_5$	2071	1973	1965		669	653	490				
	$Co(CO)_4$	2066	2003	1977	1950	550	545					
	$Cr(CO)_3Cp$	1964	1888	1870		635		580	535		855	830
	$Mo(CO)_3Cp$	1976	1892	1874		595		495	475		855	815
	$W(CO)_3Cp$	1973	1885	1869		590		520	480		855	820

[a] 1% dispersion in CsI pellets. [b] CH stretching of the cyclopentadienyl group.

However, the general assignment is not clear-cut and must be specified in each complex. The assignments were made by using the calculated force constants[27] summarized in Table V and also by comparison with data from ref 28 and 29.

The two highest vibrational frequencies can be attributed to A′ modes, with A″ having the lowest frequency. Moreover, the residual charge density calculated with the middle frequency[29,30] shows that a density of about 0.3 electron is localized on the $M(CO)_3Cp$ group. Thus, these data agree well with a covalent metal–metal bond and Graham's coefficients[31] ($\Delta\sigma$, −0.94 to −1.13; $\Delta\pi$, 0.13–0.4) confirm the presence of a single covalent metal–metal bond. In the solid state the ν_{CO} bands at the lowest wavenumber are slightly shifted (see Table VI and Figure 1). Comparison with literature data[31-35] allows assignment of the ν_{MCO} and ν_{MC} modes. The ν_{MCO} vibrations appear in the range 580–650 cm^{-1}, and the ν_{MC} bands appear in the region 475–580 cm^{-1}. Bands at 820 and 1350 cm^{-1} (this last band is not observed for all complexes) involve the C–H bond which is perpendicular to the plane of the cyclopentadienyl ring.[30,32,36,37]

All of the infrared bands of the cyclopentadienyl group could not be characterized because the porphyrin ring has stretching vibrations in this same region. However, Fritz[36-38] reports that the ν_{CH} stretching bands shift to higher wavenumbers when the metal formal oxidation state increases. Depending on the axial ligand, a ν_{CH} shift of about 200 cm^{-1} is observed (between 690 and 810–830 cm^{-1}) upon going from $[M(CO)_3Cp]^-$ to $(P)InM(CO)_3Cp$, and this suggests that the formal oxidation state of indium changes from III in (P)InCl to II in $(P)InM(CO)_3Cp$.

The local symmetry of the $Co(CO)_4$ moiety in $(P)InCo(CO)_4$ should be C_{3v}.[32,39-41] This is shown by the appearance of three bands attributed to ν_{CO} in THF solutions. The stretching and bending modes of this symmetry group are $2A_1 + E$. Calculation of the stretching force constants (see Table V) enables assignment of the highest wavenumber vibration to A_1 and the lowest wavenumber vibration to E. However, more than three bands are observed in solution (see Table VI), and this suggests a modifi-

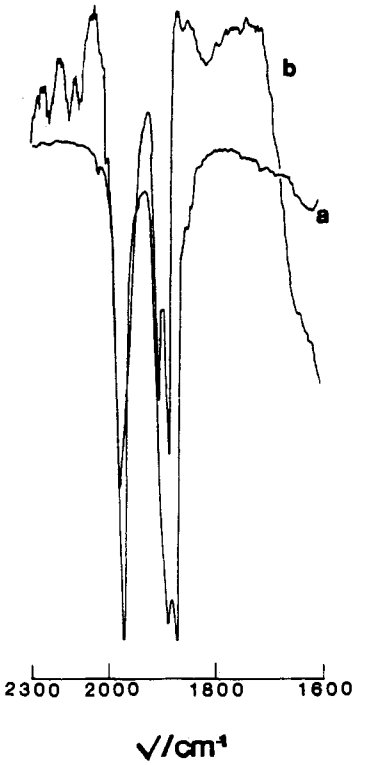

Figure 1. IR spectra of $(OEP)InMo(CO)_3Cp$ recorded (a) in THF and (b) as a 1% dispersion in CsI pellet.

(29) Kahn, O.; Bigorgne, M. *J. Organomet. Chem.* **1967**, *10*, 137.
(30) Dehand, J.; Pfeffer, M. *J. Organomet. Chem.* **1976**, *104*, 377.
(31) Graham, W. A. G. *Inorg. Chem.* **1968**, *7*, 315.
(32) Braunstein, P.; Dehand, J. *Bull. Soc. Chim. Fr.* **1975**, 1997.
(33) Parker, D. J. *J. Chem. Soc. A* **1970**, 1382.
(34) Parker, D. J. *J. Chem. Soc., Dalton Trans.* **1974**, 155.
(35) Young, C. G.; Broomhead, J. A.; Boreham, C. J. *J. Organomet. Chem.* **1984**, *260*, 91.
(36) King, R. B. *Inorg. Chim. Acta* **1968**, *2*, 454.
(37) Nakamoto, K. *Infrared and Raman Spectra of Inorganic and Coordination Compounds*, 3rd ed.; Wiley: New York, 1978; Part III, and references therein.
(38) Fritz, H. P. *Adv. Organomet. Chem.* **1964**, *1*, 239.
(39) Patmore, D. J.; Graham, W. A. G. *Inorg. Chem.* **1966**, *5*, 1586.
(40) Patmore, D. J.; Graham, W. A. G. *Inorg. Chem.* **1967**, *6*, 981.
(41) Coffey, C. E.; Lewis, J.; Nyholm, R. S. *J. Chem. Soc.* **1964**, 1741.

Table VII. UV–Visible Data of (P)InM(L) Complexes in Benzene (λ, nm; $10^{-3}\epsilon$, mol^{-1} L cm^{-1})

		λ_{max} ($10^{-3}\epsilon$)					
		Soret region		Q bands			
porphyrin, P	ligand, M(L)	I	II				ϵ(II)/ϵ(I)
TPP	$Mn(CO)_5$	387 (26.6)	457 (66.6)	544 (0.3)	586 (2.7)	633 (4.1)	2.50
	$Co(CO)_4$	369 (17.1)	446 (160.4)	534 (1.0)	575 (8.2)	618 (7.4)	9.38
	$Cr(CO)_3Cp$	393 (61.9)	459 (82.0)	547 (0.7)	588 (5.4)	636 (8.7)	1.32
	$Mo(CO)_3Cp$	383 (41.0)	457 (141.0)	542 (0.8)	587 (7.1)	634 (10.7)	3.44
	$W(CO)_3Cp$	374 (29.3)	456 (142.0)	546 (1.2)	587 (7.5)	634 (11.0)	4.85
OEP	$Mn(CO)_5$	377 (60.5)	449 (37.9)	560 (9.9)	593 (2.7)		0.63
	$Co(CO)_4$	370 (47.3)	435 (104.0)	553 (14.9)	588 (8.3)		2.20
	$Cr(CO)_3Cp$	378 (74.5)	451 (42.1)	564 (14.7)	594 (3.9)		0.57
	$Mo(CO)_3Cp$	372 (58.2)	448 (61.5)	563 (13.3)	595 (3.1)		1.06
	$W(CO)_3Cp$	370 (44.6)	448 (66.1)	563 (12.9)	595 (3.2)		1.48

cation of the local symmetry. The IR spectra of these complexes have four bands in the ν_{CO} region. This agrees with the C_s local symmetry, which predicts four IR and Raman modes. The ν_{CoCO} mode gives vibrations in the range 545–550 cm^{-1}, and the vibration close to 480 cm^{-1} for (TPP)InCo(CO)$_4$ is attributed to the ν_{CoC} mode.[30,32]

The most interesting IR spectra are obtained for the manganese complexes. These IR spectra have two bands in the carbonyl stretching region. The intensity of the highest wavenumber band is much lower than the intensity of the second band. The number of vibrations is in agreement with a C_{4v} local symmetry[42,43] although the stretching and bending modes of this group are 2 A_1 + E. The absence of one band must result from the superposition of A_1 and E modes. Such a characteristic has been already reported,[31] and calculated stretching force constants (Table V) confirm this analysis. The carbonyl regions of the solid-state IR spectra show a modification of the local symmetry and agree with a C_s symmetry. Three or four bands are observed. An assignment of ν_{MnCO} and ν_{MnC} modes was made: ν_{MnCO} in the range 635–670 cm^{-1} and ν_{MnC} at 490 cm^{-1}.[43-46] The small shift in frequency between the octaethylporphyrin and tetraphenylporphyrin complexes is due to the electron donor character of the octaethylporphyrin macrocycle which increases the electron density on the indium and results in a small shift of the ν_{CO} bands toward lower frequencies.

Data from the electronic absorption spectra of each complex are summarized in Table VII. In contrast to (P)InCl, all of the (P)InM(L) complexes have electronic absorption spectra belonging to the hyper class.[47] The Soret band involves a $\pi \rightarrow \pi^*$ electronic transition and is red-shifted (435–459 nm) in comparison to bands of (P)InCl complexes with the same porphyrin ring (see Figure 2). The extra absorption band in the near-UV region involves a charge transfer from the metal to the macrocycle ($a_{2u}(np_z) \rightarrow e_g(\pi^*)$). This charge transfer is induced by an increase of charge density on indium, which results from an electronic transfer between the two metals. The ratios of molar absorptivities between band II and band I are given in Table VII and indicate that this charge transfer is smaller than observed for alkyl or aryl σ-bonded indium porphyrins.[48] The ϵ(II)/ϵ(I) ratio is smaller for the OEP complexes than for the TPP complexes, and this is in agreement with the ring currents of each porphyrin macrocycle.

The shapes of the UV–visible spectra agree with five-coordinate ionic indium porphyrins. The UV–visible data show that the properties of the indium–metal σ-bond in (P)InM(L) are close to those of indium–carbon σ-bonded porphyrins. In particular, a large electronic exchange occurs between the axial ligand and the indium porphyrin, and a formal In(II) oxidation state is suggested.

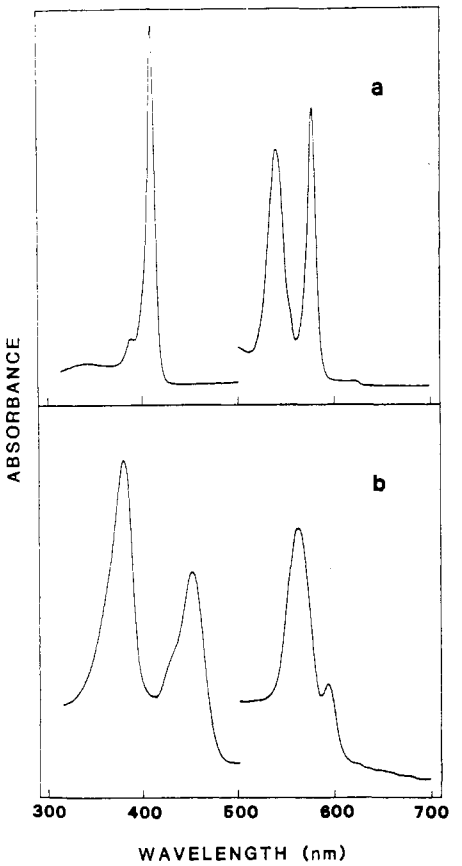

Figure 2. UV–visible spectra of (a) (OEP)InCl and (b) (OEP)InMn(CO)$_5$ in C_6H_6.

The spectral properties of pure (P)InM(L) complexes are listed in Table VII. However, another absorption band may appear in the 400–430-nm range.[17] Specifically all of the octaethyl derivatives may have another band at around 406 nm and all of the tetraphenylporphyrin complexes may have an additional band at around 427 nm, independent of the axial ligand. These additional absorptions are of variable intensity and are not observed for all the compounds. Moreover, after irradiation by light, the intensity of these bands increases. This is due to a decomposition of the bimetallic complex by cleavage of the indium–metal bond, and the absorptions at 406 or 427 nm correspond to the Soret band of $[(P)In]^+$.

A ^1H NMR study was made on the same series of complexes in C_6D_6 at ambient temperature, and the chemical shifts are summarized in Table VIII. All of the complexes exhibit ^1H NMR features typical of diamagnetic metalloporphyrins.

The NMR spectra are analogous between the binuclear systems and their (P)InCl precursors. The pyrrole protons of (TPP)InM(L) have a signal at ~9.09 ppm except for the (TPP)In-

(42) Cotton, F. A.; Kraihanzel, C. S. *J. Am. Chem. Soc.* **1962**, *84*, 4432.
(43) Braunstein, P.; Dehand, J. *J. Organomet. Chem.* **1974**, *81*, 123.
(44) Hsieh, A. T. T.; Mays, M. J. *J. Chem. Soc., Dalton Trans.* **1972**, 516.
(45) Wilford, J. B.; Stone, F. G. A. *Inorg. Chem.* **1965**, *4*, 389.
(46) Kasenally, A. S.; Lewis, J.; Manning, A. R.; Miller, J. R.; Nyholm, R. S.; Stiddard, M. H. B. *J. Chem. Soc.* **1965**, 3407.
(47) Gouterman, M. In *The Porphyrins*; Dolphin, D., Ed.; Academic: New York, 1978; Vol. III, Chapter 1, and references therein.
(48) Kadish, K. M.; Boisselier-Cocolios, B.; Cocolios, P.; Guilard, R. *Inorg. Chem.* **1985**, *24*, 2139.

Table VIII. ^{1}H NMR Data of (P)InCl and (P)InM(L) Complexes[a]

porphyrin, P	axial ligand	R_1	R_2	protons of R_1			protons of R_2		protons of axial ligand	
					mult/i[b]	δ		mult/i[b]	δ	mult/i[b]	δ
TPP	Cl	C_6H_5	H	*o*-H	m/4	8.02		s/8	9.04		
				o'-H	m/4	7.98					
				m-H, *p*-H	m/12	7.45					
	$Mn(CO)_5$	C_6H_5	H	*o*-H	m/4	8.35		s/8	9.09		
				o'-H	m/4	8.07					
				m-H, *p*-H	m/12	7.49					
	$Co(CO)_4$	C_6H_5	H	*o*-H	m/4	8.54		s/8	9.30		
				o'-H	m/4	8.32					
				m-H, *p*-H	m/12	7.64					
	$Cr(CO)_3Cp$	C_6H_5	H	*o*-H	m/4	8.51		s/8	9.08	s/5	1.84
				o'-H	m/4	8.03					
				m-H, *p*-H	m/12	7.47					
	$Mo(CO)_3Cp$	C_6H_5	H	*o*-H	m/4	8.45		s/8	9.09	s/5	2.59
				o'-H	m/4	8.03					
				m-H, *p*-H	m/12	7.47					
	$W(CO)_3Cp$	C_6H_5	H	*o*-H	m/4	8.46		s/8	9.09	s/5	2.53
				o'-H	m/4	8.02					
				m-H, *p*-H	m/12	7.47					
OEP	Cl	H	C_2H_5		s/4	10.39	β-CH_3	t/24	1.83		
							α-CH_2	m/8	3.88		
							α'-CH_2	m/8	4.03		
	$Mn(CO)_5$	H	C_2H_5		s/4	10.45	β-CH_3	t/24	1.88		
							α-CH_2	m/16	4.04		
	$Co(CO)_4$	H	C_2H_5		s/4	10.48	β-CH_3	t/24	1.87		
							α-CH_2	m/16	4.03		
	$Cr(CO)_3Cp$	H	C_2H_5		s/4	10.45	β-CH_3	t/24	1.87	s/5	1.63
							α-CH_2	m/8	3.98		
							α'-CH_2	m/8	4.08		
	$Mo(CO)_3Cp$	H	C_2H_5		s/4	10.45	β-CH_3	t/24	1.87	s/5	2.39
							α-CH_2	m/8	3.99		
							α'-CH_2	m/8	4.09		
	$W(CO)_3Cp$	H	C_2H_5		s/4	10.43	β-CH_3	t/24	1.87	s/5	2.35
							α-CH_2	m/8	3.99		
							α'-CH_2	m/8	4.09		

[a] Spectra recorded in C_6D_6 at 21 °C with $SiMe_4$ as internal reference; chemical shifts (δ) downfield from $SiMe_4$ are defined as positive. [b] Legend: mult = multiplicity; i = intensity; s = singlet; t = triplet; m = multiplet.

$Co(CO)_4$ complex at 9.30 ppm (see Table VIII), and this may be compared to 9.04 ppm for (TPP)InCl. No significant differences in signal position can be observed for the other protons. This reflects a weak influence of the axial ligand, thus implying a large distance from the nuclear center of the macrocycle.

The chemical shifts of the phenyl protons give more structural information. The meta and para protons have resonances in the range 7.47–7.64 ppm. The ortho protons of (TPP)InM(L) are not equivalent as is the case for (TPP)InCl.[49,50] This lack of equivalence results in an asymmetry with respect to the porphyrin plane and has its origin in the symmetry of the (TPP)InM(L) complexes. The axial metalate ion induces a larger nonequivalence of the two porphyrin faces[49-52] in comparison to parameters of (TPP)InCl ($|\delta_{o'\text{-H}} - \delta_{o\text{-H}}| = 0.04$ ppm). This is due to a slower rotation of the phenyl groups on the NMR time scale ($|\delta_{o'\text{-H}} - \delta_{o\text{-H}}| = 0.28$ ((TPP)InMn(CO)$_5$), 0.22 ((TPP)InCo(CO)$_4$), 0.42 ((TPP)InMo(CO)$_3$Cp), 0.44 ((TPP)InW(CO)$_3$Cp), 0.48 ((TPP)InCr(CO)$_3$Cp)). The ortho protons of the (TPP)InM(CO)$_3$Cp derivatives are the most inequivalent, and this can be attributed to a steric effect of the cyclopentadienyl group. When the macrocycle is octaethylporphyrin, the resonance signals invariably appear at lower fields than those of (OEP)InCl ($\Delta\delta$ = 0.6 ppm). The meso protons give a signal close to 10.43–10.48 ppm whereas the methylenic and methylic protons appear in the ranges 4.03–4.09 and 1.87–1.88 ppm (3.95 (average) and 1.83 ppm for (OEP)InCl). The deshielding is attributable to the slightly higher electron-withdrawing character of the metalate anion compared to that of the chloride ion.

When the indium atom is coordinated to a [M(CO)$_3$Cp] axial ligand, two multiplets are clearly observed for the methylenic protons, and this results from a ABX_3 coupling with the methylic protons. The difference between the resonance frequencies of the methylenic protons, $|\nu_A - \nu_B|$, shows that the Cr(CO)$_3$Cp ligand is the most anisotropic ligand (37.18 Hz (Mo(CO)$_3$Cp) $\leq$ 37.87 Hz (W(CO)$_3$Cp) $<$ 41.81 Hz (Cr(CO)$_3$Cp)). The same classification can be obtained by considering the difference between the two ortho proton chemical shifts of the tetraphenylporphyrin derivatives, $|\delta_{o'\text{-H}} - \delta_{o\text{-H}}|$. An ABX_3 coupling is also observed between the two methylenic protons of (OEP)InCo(CO)$_4$ and (OEP)InMn(CO)$_5$, but the anisotropy is smaller. This implies a small separation of indium from the plane of the porphyrin macrocycle. These observations are in good agreement with the symmetry of the axial ligand; the more symmetrical the axial ligand ($C_s \rightarrow C_{3v} \rightarrow C_{4v}$), the lower the anisotropy of the methylene protons.

The shielding of the cyclopentadienyl ligand is very strong compared to that in other organometallic derivatives. This shielding is in good agreement with the ring current of the porphyrin macrocycle and results in a higher shielding of the protons

(49) Abraham, R. J.; Smith, K. M. *Tetrahedron Lett.* **1971**, *36*, 3335.
(50) Janson, T. R.; Katz, J. J. In *The Porphyrins*; Dolphin, D., Ed.; Academic: New York, 1978; Vol. IV, Chapter 1, and references therein.
(51) Scheer, H.; Katz, J. J. In *Porphyrins and Metalloporphyrins*; Smith, K. M., Ed.; Elsevier Scientific: Amsterdam, 1975; Chapter 10, and references therein.
(52) Busby, C. A.; Dolphin, D. *J. Magn. Reson.* **1976**, *23*, 211.

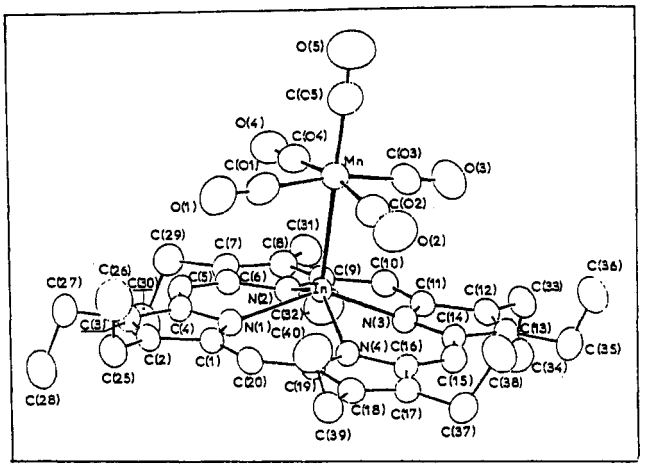

Figure 3. ORTEP drawing and labeling scheme for $(OEP)InMn(CO)_5$.

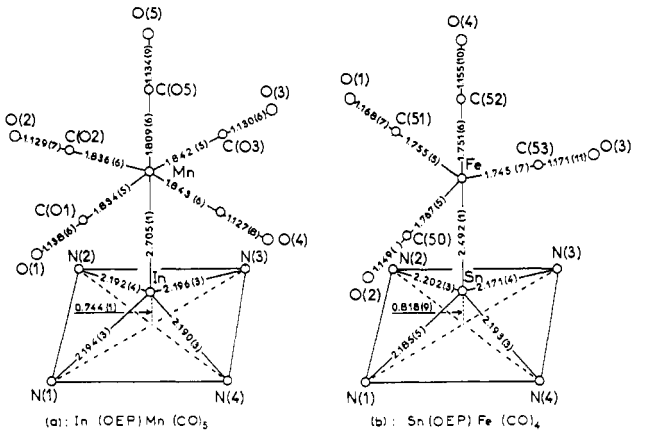

Figure 4. Coordination polyhedrons of (a) $(OEP)InMn(CO)_5$ and (b) $(OEP)SnFe(CO)_4$.

on the cyclopentadienyl ligand of the more basic OEP complexes. (1.84–2.59 ppm for the TPP complexes and 1.63–2.39 ppm for the OEP complexes). The smaller the metal–macrocycle distance, the higher will be the shielding of the axial ligand protons. (For example, the value is 1.84 ppm for $(TPP)InCr(CO)_3Cp$ and 2.53 ppm for $(TPP)InW(CO)_3Cp$.)

Molecular Structure Description. Figure 3 gives an ORTEP view of the $(OEP)InMn(CO)_5$ complex and the numbering scheme used. Figure 4 and Table IX give the bond distances within the coordination polyhedron. $(OEP)InMn(CO)_5$ has two metal units, which are linked by a single covalent bond. The In–Mn distance is 2.705 (1) Å. As expected, this metal–metal bond length is much longer than the metal–metal bond length observed in $(OEP)SnFe(CO)_4$[14] (Sn–Fe = 2.492 (1) Å). Figure 4 compares the coordination polyhedron of the two crystal structures. Both the indium and the tin atoms are five-coordinated by the porphyrin macrocycle and the metal carbonyl unit. The average metal–nitrogen distances for the indium and tin compounds are 2.193 (2) and 2.118 (11) Å, respectively, whereas the metal is out of the plane of the four nitrogens by 0.744 (1) and 0.818 (9) Å, respectively. The manganese atom in $(OEP)InMn(CO)_5$ is almost on the fourfold axis of the porphyrin molecule (N_i–In–Mn = 109.8 ± 0.9°, i = 1.4).

The equatorial carbonyl ligands linked to the manganese or the iron atoms are bent toward the porphyrin unit in both structures (⟨C–Mn–In⟩ = 83.8 (5)°, ⟨C–Fe–Sn⟩ = 87.2 (6)°). This doming is larger for the manganese complex and is equal to that found in the neutron structure of $HMn(CO)_5$[53] (⟨C–Mn–H⟩ = 82.8 (8)°).

(53) La Placa, S. J.; Hamilson, W. C.; Ibers, J. A.; Davison, J. A. *Inorg. Chem.* **1969**, *8*, 1928.

Table IX. Bond Distances (Å), Angles (deg), and Standard Deviations in the Coordination Polyhedron and $Mn(CO)_5$ Ligand

In the Coordination Polyhedron			
In–N(1)	2.194 (3)	In–C(O1)	3.110 (6)
In–N(2)	2.192 (4)	In–C(O2)	3.113 (7)
In–N(3)	2.196 (3)	In–C(O3)	3.110 (4)
In–N(4)	2.190 (3)	In–C(O4)	3.077 (4)
N(1)–N(3)	4.136 (4)	N(2)–N(4)	4.115 (5)
In–Mn	2.705 (1)		
N(1)–In–Mn	110.29 (9)	N(1)–In–N(2)	83.3 (1)
N(2)–In–Mn	110.10 (7)	N(2)–In–N(3)	83.4 (1)
N(3)–In–Mn	108.90 (8)	N(3)–In–N(4)	83.5 (1)
N(4)–In–Mn	110.0 (1)	N(4)–In–N(1)	83.3 (1)
In–Mn–C(O1)	84.2 (2)	In–Mn–C(O2)	84.2 (2)
In–Mn–C(O3)	84.0 (2)	In–Mn–C(O4)	82.8 (2)
In the $Mn(CO)_5$ Ligand			
Mn–C(O1)	1.834 (5)	C(O1)–O(1)	1.138 (6)
Mn–C(O2)	1.836 (6)	C(O2)–O(2)	1.129 (7)
Mn–C(O3)	1.842 (5)	C(O3)–O(3)	1.130 (6)
Mn–C(O4)	1.843 (6)	C(O4)–O(4)	1.127 (8)
Mn–C(O5)	1.809 (6)	C(O5)–O(5)	1.134 (9)
C(O1)–Mn–C(O2)	89.2 (2)	C(O1)–Mn–C(O5)	96.3 (3)
C(O1)–Mn–C(O3)	168.2 (3)	C(O2)–Mn–C(O5)	96.2 (3)
C(O2)–Mn–C(O4)	167.0 (3)	C(O3)–Mn–C(O5)	95.5 (2)
C(O2)–Mn–C(O3)	89.2 (2)	C(O4)–Mn–C(O5)	96.7 (3)
C(O3)–Mn–C(O4)	90.1 (2)	C(O4)–Mn–C(O1)	88.8 (2)
Mn–C(O4)–O(1)	178.5 (6)	Mn–C(O2)–O(2)	177.4 (6)
Mn–C(O3)–O(3)	177.8 (4)	Mn–C(O4)–O(4)	180.0 (1)

The torsional angles (N_i–In–Mn–C) of $(OEP)InMn(CO)_5$ are given in the supplementary material. The equatorial carbonyl groups in $(OEP)InMn(CO)_5$ do not exactly eclipse the four In–N bonds. The average Mn–C equatorial distance (1.839 (4) Å) is longer than the axial one (1.809 (6) Å). This observation is in agreement with previous structural data related to metal carbonyls.[54,55] Consequently, it can be deduced that the CO ligand has a larger trans effect than the (OEP)In unit. This trans effect is not present for $(OEP)SnFe(CO)_4$. The bond distances and angles in the macrocycle agree well with those usually described for other OEP complexes.[2] The doming character of the porphyrin ligand is equal to 0.07 Å. According to Wayland[12] it is possible to calculate the M–M′ bond length of (P)MM′(P) from the individual covalent radii. If one uses the covalent radius of 1.39 Å[56] for the manganese atom and calculates an indium radius of 1.36 Å from $(TPP)In(CH_3)$[57] ($In–CH_3$ = 2.13 Å, r_c = 0.77 Å), then the In–Mn single covalent bond should have a bond length of 1.39 + 1.36 = 2.75 Å. This value agrees well with the experimental value of 2.705 (1) Å.

Reduction of (OEP)InM(L) and (TPP)InM(L). Each (OEP)InM(L) complex undergoes one reduction in the potential range of CH_2Cl_2. This is in contrast to (TPP)InM(L), which has a less basic porphyrin ring and is reduced in two single-electron-transfer steps in CH_2Cl_2.

All of the electroreductions are characterized by an instability of the singly and doubly reduced species. This was first shown for $(TPP)InM(CO)_3Cp$, where M = Mo, W,[19] and is also true for the other (P)InM(L) complexes investigated in this study.

Cyclic voltammograms of $(OEP)InMn(CO)_5$, $(OEP)InMo(CO)_3Cp$, and $(OEP)InCo(CO)_4$ are illustrated in Figure 5. The peak current of each reduction is proportional to the square root of the scan rate, indicating a diffusion-controlled process. A well-defined voltammogram with $|E_{pa} - E_{pc}| = 60 \pm 10$ mV is obtained for $(OEP)InMn(CO)_5$ and $(OEP)InMo(CO)_3Cp$, but not for $(OEP)InCo(CO)_4$, which undergoes a rapid cleavage of the indium–metal bond after electroreduction.

(54) Martin, M.; Rees, B.; Mitschler, A. *Acta Crystallogr., Sect. B: Struct. Crystallogr. Cryst. Chem.* **1982**, *B38*, 1286.
(55) Zhu, N. J.; Lecomte, C.; Coppens, P.; Keistler, J. P. *Acta Crystallogr., Sect. B: Struct. Crystallogr. Cryst. Chem.* **1982**, *B38*, 1286.
(56) Cotton, F. A.; Richardson, D. C. *Inorg. Chem.* **1966**, *5*, 1851.
(57) Lecomte, C.; Protas, J.; Cocolios, P.; Guilard, R. *Acta Crystallogr., Sect. B: Struct. Crystallogr. Cryst. Chem.* **1980**, *B36*, 2769.

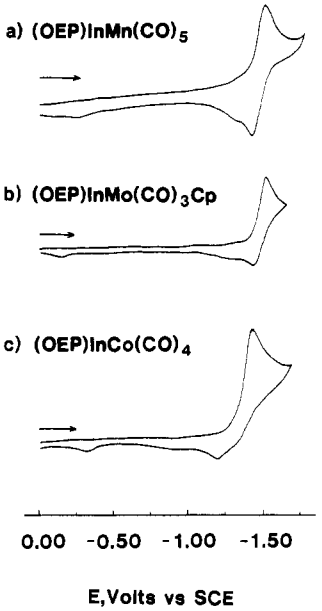

Figure 5. Cyclic voltammograms for the reduction of (a) (OEP)InMn-$(CO)_5$, (b) (OEP)InMo$(CO)_3$Cp, and (c) (OEP)InCo$(CO)_4$ in CH_2Cl_2 containing 0.1 M (TBA)PF_6. The scan rate was 0.20 V/s.

The stability of each singly reduced $[(P)InM(L)]^{\bullet-}$ complex is related to the reversibility of the reduction process at room temperature and can be estimated from the ratio of the anodic to cathodic peak currents, which varied as a function of the M(L) group bound to (TPP)In and decreased in the order

$$Mn(CO)_5 > W(CO)_3Cp > Mo(CO)_3Cp > Cr(CO)_3Cp > Co(CO)_4$$

The same order of compound stability is obtained for (TPP)-InM(L) and (OEP)InM(L). The observed trend with M(L) also follows an order of increasing nucleophilicity given for the reaction of $[M(L)]^-$ with RX.[58]

Half-wave and peak potentials for the reduction of (OEP)-InMn$(CO)_5$ and (TPP)InMn$(CO)_5$ were invariant with an increase in potential scan rate, but peak potentials for reduction of the other (OEP)InM(L) and (TPP)InM(L) complexes shifted by −30 mV for each 10-fold increase in scan rate. This potential shift is consistent with an irreversible chemical reaction that follows a reversible one-electron-transfer process.[59]

The irreversible chemical reaction coupled to the electroreduction corresponds to a cleavage of the (P)InM(L) indium–metal bond, the rate of which decreases as the temperature of the solution is lowered. This is illustrated in Figure 6 for the reduction of (TPP)InMo$(CO)_3$Cp and (TPP)InCr$(CO)_3$Cp in CH_2Cl_2.

As seen in Figure 6, five anodic peaks are observed after the stepwise reduction of (TPP)InMo$(CO)_3$Cp or (TPP)InCr$(CO)_3$Cp by two electrons. Two of these peaks correspond to an oxidation of electrogenerated $[(TPP)InM(L)]^{2-}$ and $[(TPP)InM(L)]^{\bullet-}$ while the other three peaks can be assigned as oxidation of $[(P)In]^-$ and $(P)In^{\bullet}$ or the anionic metalate fragments generated upon cleavage of the indium–metal bond.[19]

Peak potentials for oxidation of $[(TPP)In]^-$ and $(TPP)In^{\bullet}$ occur at $E_p = -1.43$ and −1.04 V, and anodic processes at these two potentials are seen in Figure 6. Peak potentials for oxidation of $[Mo(CO)_3Cp]^-$ and $[Cr(CO)_3Cp]^-$ occur at $E_p = -0.14$ and −0.28 V in CH_2Cl_2, and these processes are also observed in parts a and b of Figure 6.

A decomposition of $[(OEP)InCo(CO)_4]^{\bullet-}$ occurs before the complex can be further reduced (see Figure 5c). The $[(TPP)-InCo(CO)_4]^{\bullet-}$ derivative shows the same behavior, but a second reduction of the other (TPP)InM(L) complexes is possible. These half-wave potentials and peak potentials are listed in Table X,

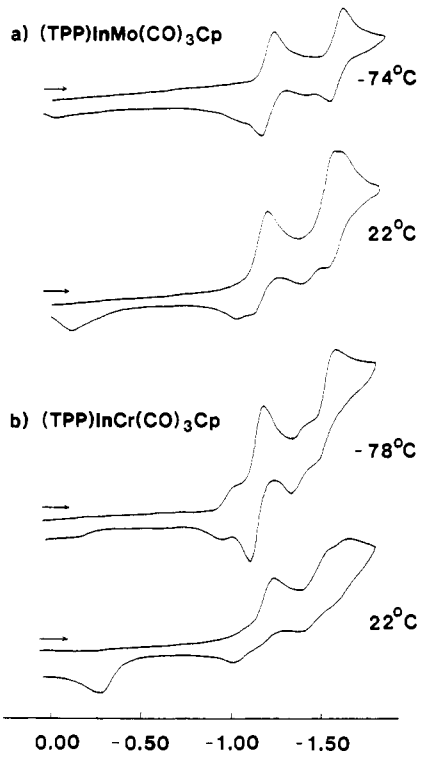

Figure 6. Cyclic voltammograms of (a) (TPP)InMo$(CO)_3$Cp and (b) (TPP)InCr$(CO)_3$Cp in CH_2Cl_2 containing 0.1 M (TBA)PF_6 at low temperature and at room temperature. The scan rate was 0.10 V/s.

Table X. Peak Potentials (E_p at 0.20 V/s) and Half-Wave Potentials ($E_{1/2}$, V vs. SCE) of (P)InM(L) in CH_2Cl_2 Containing 0.1 M (TBA)PF_6

porphyrin, P	ligand, m(L)	oxidn				redn[d]	
		E_{pa}	E_{pa}[b]	$E_{1/2}$[c]		$E_{1/2}$	
(TPP)In	none[a]			1.20	1.51	−1.08	−1.48
	$Mn(CO)_5$	0.80		1.20	1.51	−1.17	−1.62
	$Co(CO)_4$	0.91	1.01	1.20	1.52	−1.18[e]	
	$W(CO)_3Cp$	0.76	0.97	1.20	1.51	−1.23	−1.66[e]
	$Mo(CO)_3Cp$	0.79	0.99	1.21	1.51	−1.20	−1.63[e]
	$Cr(CO)_3Cp$	0.74		1.20	1.51	−1.22[e]	−1.66[e]
(OEP)In	none			1.13	1.48	−1.31	−1.78
	$Mn(CO)_5$	0.76		1.13	1.47	−1.46	
	$Co(CO)_4$	0.82	1.01	1.13	1.48	−1.41[e]	
	$W(CO)_3Cp$	0.69	0.97	1.13	1.48	−1.49	
	$Mo(CO)_3Cp$	0.74	0.99	1.14	1.48	−1.48	
	$Cr(CO)_3Cp$	0.67		1.13	1.47	−1.47[e]	

[a] Neutral monomeric complex present as (P)InPF_6. [b] Corresponds to oxidation of $[M(L)]_2$. [c] Corresponds to reversible oxidations of (P)In-PF_6. [d] Only reductions of (P)InM(L) are shown. Additional reductions of $[(P)In]^+$ and (P)In occur at $E_{1/2} = -1.08$ and −1.48 V (TPP) or −1.31 and −1.78 V (OEP). [e] Value of E_{pc} at 0.20 V/s.

Scheme I

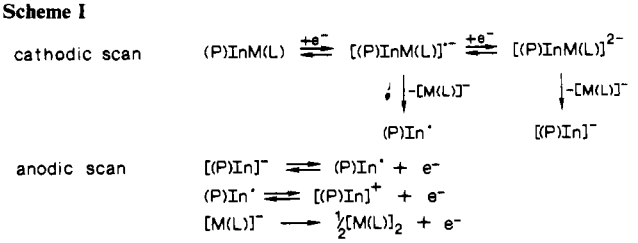

and the overall reduction/oxidation sequence involving (P)InM(L) is given in Scheme I.

The reduction of (P)InM(L) can occur by one or two electrons, depending upon the specific porphyrin ring, the temperature, and

(58) Dessy, R. E.; King, R. B.; Waldrop, M. *J. Am. Chem. Soc.* **1966**, *88*, 5112.
(59) Nicholson, R. S.; Shain, I. *Anal. Chem.* **1964**, *36*, 706.

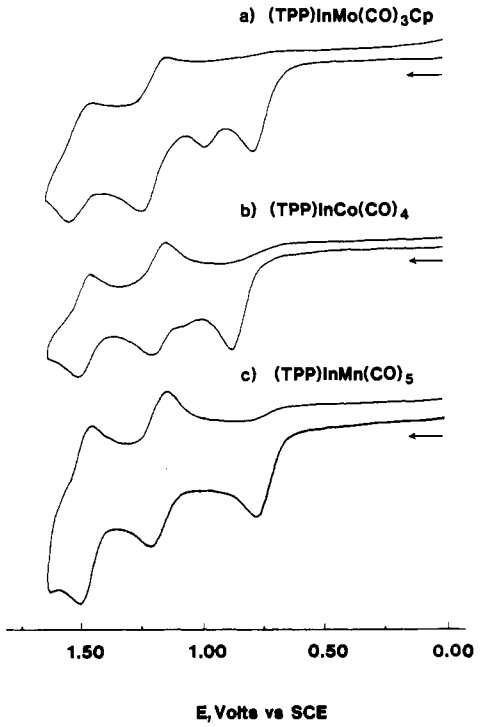

Figure 7. Cyclic voltammograms for the oxidation of (a) (TPP)InMo(CO)$_3$Cp, (b) (TPP)InCo(CO)$_4$, and (c) (TPP)InMn(CO)$_5$ in CH_2Cl_2 containing 0.1 M (TBA)PF_6. The scan rate was 0.20 V/s.

the nature of the bound metalate ion. Potentials for these reactions are listed in Table X. Additional oxidation and reduction peaks may also be observed for (TPP)In$^{\bullet}$ and [(TPP)In]$^-$, which are formed after cleavage of the reduced bimetallic complex, as well as for [(TPP)In]$^+$ reduction and oxidation when some decomposition of the neutral complex occurs. These potentials are not listed in Table X, but the processes are evident from the voltammograms in Figures 5 and 6.

No electrochemistry of generated [M(L)]$^-$ was observed on the reductive potential sweep, but the oxidation of this anionic fragment could easily be detected on reversal of the potential. This is evident in Figures 5 and 6, where oxidations are observed at E_p = –0.22 V ([Mn(CO)$_5$]$^-$), –0.14 V ([Mo(CO)$_3$Cp]$^-$), or –0.28 V ([Cr(CO)$_3$Cp]$^-$). These processes have been identified by independent studies[60–63] of these anionic species, and the oxidation corresponds to the reaction

$$[M(L)]^- \rightarrow {}^1/_2[M(L)]_2 + e^-$$

An additional oxidation peak is also observed at E_p = –0.30 V after reduction of (TPP)InCo(CO)$_4$. This oxidation peak is not due to [Co(CO)$_4$]$^-$, which is oxidized at +0.40 V, but rather to oxidation of another cobalt carbonyl fragment.

No evidence of an M(L) radical was detected upon decomposition of (P)InM(L). This lack of an observed radical intermediate under all experimental conditions clearly suggests the decomposition pathway shown in Scheme I. Several attempts were made to characterize reduced [(P)InM(L)]$^{\bullet-}$ and [(P)InM(L)]$^{2-}$ by spectroelectrochemical techniques. However, these spectral methods were generally unsuccessful and only indicated mixtures of the monomeric and bimetallic indium porphyrin in solution.

It was initially proposed that (TPP)InW(CO)$_3$Cp was reduced at the W(CO)$_3$Cp group,[19] but combined electrochemical and spectroelectrochemical data of several different (P)InM(L) complexes now indicate that the site of the first electron transfer is not that clear-cut. The reduction potentials of (P)InM(L) are similar to potentials of the indium–carbon-σ-bonded complexes,[48,64] where reduction occurs at the porphyrin π ring system. Also, potential separations between the two one-electron reductions of (TPP)InM(L) range between 0.40 and 0.45 V, thus further suggesting the formation of anion radicals and dianions[65] before cleavage of the metal–metal bond.

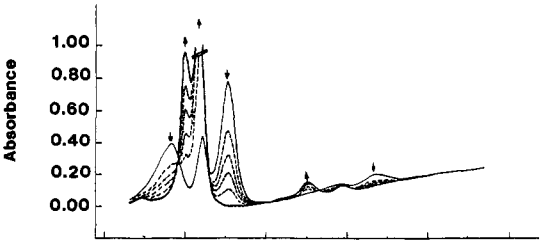

Figure 8. Time-resolved electronic absorption spectra taken during oxidation of (TPP)InMn(CO)$_5$ in CH_2Cl_2 containing 0.1 M (TBA)PF_6. The initial and final spectra are represented by solid lines.

Scheme II

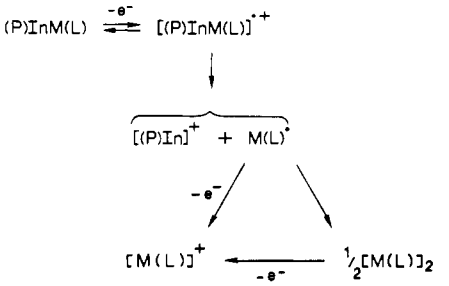

Oxidation of (P)InM(L). Cyclic voltammograms of (TPP)InMo(CO)$_3$Cp, (TPP)InCo(CO)$_4$, and (TPP)InMn(CO)$_5$ are illustrated in Figure 7. As seen in this figure, each bimetallic complex has one or two irreversible anodic peaks, which are followed by two reversible processes at more positive potentials. Similar current–voltage curves were observed for oxidation of the other (TPP)InM(L) and (OEP)InM(L) complexes, and peak potentials and half-wave potentials for these processes are given in Table X.

The first oxidation of (P)InM(L) occurs at peak potentials between 0.67 and 0.91 V. This oxidation is not coupled to a reverse reduction at any scan rate up to 200 V/s or at temperatures as low as –78 °C. $|E_p - E_{p/2}| = 66 \pm 4$ mV and the constant $i_p/v^{1/2}$ ratio at room temperature indicate that the abstraction of one electron is diffusion-controlled but that a rapid cleavage of the metal–metal bond follows oxidation.

The electrooxidation of each (P)InM(L) complex was monitored by variable-scan and variable-temperature electrochemistry as well as by ESR spectroscopy and spectroelectrochemistry. A combination of results from these studies leads to the postulated sequence of electron-transfer steps shown in Scheme II.

In Scheme II, (P)InM(L) is reversibly oxidized by one electron to give [(P)InM(L)]$^{\bullet+}$. This oxidized bimetallic complex then undergoes a rapid cleavage of the metal–metal bond to generate [(P)In]$^+$ and M(L)$^{\bullet}$ in solution. The generated M(L) radical may dimerize to give [M(L)]$_2$[60,62] or it may be oxidized directly to [M(L)]$^+$.

(60) Kadish, K. M.; Lacombe, D. A.; Anderson, J. E. *Inorg. Chem.* **1986**, *25*, 2246 and references therein.
(61) Pickett, C. J.; Pletcher, D. *J. Chem. Soc., Dalton Trans.* **1975**, 879.
(62) Lacombe, D. A.; Anderson, J. E.; Kadish, K. M. *Inorg. Chem.* **1986**, *25*, 2074.
(63) Madach, T.; Vahrenkamp, H. *Z. Naturforsch., B.: Anorg. Chem., Org. Chem.* **1978**, *33B*, 1301.
(64) Tabard, A.; Guilard, R.; Kadish, K. M. *Inorg. Chem.* **1986**, *25*, 4277.
(65) Kadish, K. M. *Prog. Inorg. Chem.* **1986**, *34*, 435–605.
(66) Kadish, K. M.; Cornillon, J.-L.; Cocolios, P.; Tabard, A.; Guilard, R. *Inorg. Chem.* **1985**, *24*, 3645.
(67) Wrighton, M. S.; Ginley, D. S. *J. Am. Chem. Soc.* **1975**, *97*, 4246.
(68) Lemoine, P.; Giraudeau, A.; Gross, M. *Electrochim. Acta* **1976**, *21*, 1.
(69) Hughey, J. L.; Bock, C. R.; Meyer, T. J. *J. Am. Chem. Soc.* **1975**, *97*, 4440.
(70) Wrighton, M. *Chem. Rev.* **1974**, *74*, 401.

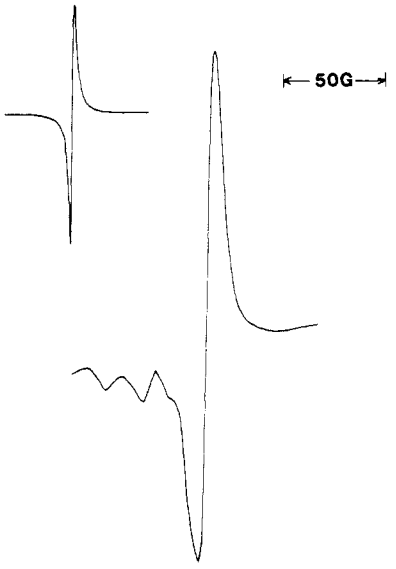

Figure 9. ESR spectrum of oxidized (TPP)InMo(CO)$_3$Cp at 120 K in CH_2Cl_2 containing 0.1 M (TBA)PF_6.

A direct oxidation of M(L)$^\bullet$ to [M(L)]$^+$ will result in increased oxidation currents for the first oxidation process, and this is illustrated in Figure 7c for (TPP)InMn(CO)$_5$. In contrast, formation of [M(L)]$_2$ results in an additional oxidation of this dimeric species. This reaction occurs in the narrow potential range 0.97–1.01 V (see Table X)[60-63] and is illustrated by the oxidation of (TPP)InMo(CO)$_3$Cp in Figure 7a.

In all cases, the ultimate (P)InM(L) oxidation products after abstraction of two electrons are [(P)In]$^+$ and [M(L)]$^+$. The [M(L)]$^+$ cation is not further oxidized, but two reversible oxidations do occur for [(P)In]$^+$.[66] Half-wave potentials for these oxidations are listed in Table X, and these reactions are illustrated by the voltammograms in Figure 7 for three representative (TPP)InM(L) complexes.

Thin-layer spectra obtained during oxidation of (TPP)InMn(CO)$_5$ are illustrated in Figure 8. Upon application of an oxidizing potential there is rapid formation of a compound whose UV–visible spectrum has a Soret band at 425 nm, a shoulder at 403 nm, and two Q bands at 557 and 597 nm. This spectrum is similar to that of (TPP)InPF_6. The same spectral evolution is obtained for each (P)InM(L) complex, and [(TPP)In]$^+$ or [(OEP)In]$^+$ is the ultimate porphyrin oxidation product. Dimeric $Mn_2(CO)_{10}$ is also formed during oxidation of (TPP)InMn(CO)$_5$, and the small peak at ~340 nm in Figure 8 is attributed to this species.[67]

The above spectroelectrochemical results are in agreement with results from cyclic voltammetry and are consistent with the mechanism shown in Scheme II. Also, the reversible oxidation waves at +1.20 V (TPP) or +1.13 V (OEP) (Figure 7 and Table X) are identical with half-wave potentials for the first and second oxidations of (P)InPF_6.[66]

Oxidized solutions of (P)InMo(CO)$_3$Cp have an ESR signal with $g = 1.955$ at 120 K in CH_2Cl_2 containing 0.1 M (TBA)PF_6. This ESR spectrum is represented in Figure 9 and is similar to spectra reported for Mo(CO)$_3$Cp$O_2^\bullet$.[68] This again suggests that cleavage of the indium–metal bond occurs as shown in Scheme II.

The electrochemical oxidation of [M(L)]$_2$, where [M(L)]$_2$ = [Mn(CO)$_5$]$_2$, [Co(CO)$_4$]$_2$, [Cr(CO)$_3$Cp]$_2$, [W(CO)$_3$Cp]$_2$, [Mo(CO)$_3$Cp]$_2$, leads to the transient formation of an M(L) radical after cleavage of the metal–metal bond.[60,63,71] An M(L) radical has also been obtained by a photochemical reaction,[67,69,72] but its dimerization rate constant is very high ($k_{dim} \geq 10^8$ M^{-1} s^{-1}) at room temperature, and the species can be observed by ESR only after trapping with O_2 in solution.[73-77] Thus, it is proposed that the ESR spectrum in Figure 9 is actually due to quantities of M(L)$O_2^\bullet$ formed during the reaction of M(L)$^\bullet$ with trace O_2 in solution.

In summary, the stability of the indium–metal-σ-bonded (P)InM(L) is relatively low. The neutral derivatives show some decomposition in solution, but the magnitude of this decomposition depends on the nature of the σ-bonded metalate group. In all cases, the addition or abstraction of one electron to bimetallic (P)InM(L) leads to a porphyrin anion or cation whose lifetime is short and varies as a function of the axial ligand. Electroreduction seems to involve the porphyrin π ring system, but participation of a σ metal-based orbital cannot be ruled out.

Acknowledgment. The support of the National Science Foundation (Grant No. CHE-8515411 and No. INT-8413696), the Robert A. Welch Foundation (K.M.K., Grant No. E-680), and the CNRS is gratefully acknowledged. We also acknowledge Panos Cocolios and Dane Chang for preliminary experiments on some of these systems.

Registry No. (TPP)InMn(CO)$_5$, 94928-90-2; (TPP)InCo(CO)$_4$, 94943-91-6; (TPP)InCr(CO)$_3$Cp, 108270-09-3; (TPP)InMo(CO)$_3$Cp, 91312-84-4; (TPP)InW(CO)$_3$Cp, 91312-85-5; (OEP)InMn(CO)$_5$, 82066-80-6; (OEP)InCo(CO)$_4$, 82066-81-7; (OEP)InCr(CO)$_3$Cp, 108270-12-8; (OEP)InMo(CO)$_3$Cp, 82496-58-0; (OEP)InW(CO)$_3$Cp, 82496-59-1; [(OEP)In]$^+$, 108270-13-9; (OEP)In, 108294-69-5; [(TPP)In]$^+$, 56551-52-1; (TPP)In, 102513-31-5; (OEP)InCl, 32125-07-8; (TPP)InCl, 63128-70-1; [Mn(CO)$_5$]$^-$, 14971-26-7; [Co(CO)$_4$]$^-$, 14971-27-8; [Cr(CO)$_3$Cp]$^-$, 48121-47-7; [Mo(CO)$_3$Cp]$^-$, 12126-18-0; [W(CO)$_3$Cp]$^-$, 12126-17-9; $Co_2(CO)_8$, 15226-74-1; [Mo(CO)$_3$Cp]$_2$, 12091-64-4; (TPP)In(CH$_3$), 63074-31-7; [(TPP)InMo(CO)$_3$Cp]$^{2-}$, 108270-14-0; [(TPP)InCr(CO)$_3$Cp]$^{2-}$, 108270-15-1; [(TPP)InMo(CO)$_3$Cp]$^-$, 108270-16-2; [(TPP)InCr(CO)$_3$Cp]$^-$, 108270-17-3; [(TPP)In]$^-$, 108270-18-4; (OEP)In(CH$_3$), 63288-51-7; In, 7440-74-6; Mn, 7439-96-5; Co, 7440-48-4; Cr, 7440-47-3; Mo, 7439-98-7; W, 7440-33-7.

Supplementary Material Available: Tables of hydrogen atom fractional coordinates, anisotropic temperature factors, bond distances and angles in the porphyrin ligand, and least-squares planes and a Newman projection of the (N_4)InMn(CO)$_5$ unit along the metal–metal bond (9 pages); a table of observed and calculated structure factors for (OEP)InMn(CO)$_5$ (45 pages). Ordering information is given on any current masthead page.

(71) Madach, T.; Vahrenkamp, H. *Z. Naturforsch., B: Anorg. Chem., Org. Chem.* **1979**, *34B*, 573.
(72) Laine, R. M.; Ford, P. C. *Inorg. Chem.* **1977**, *16*, 388.
(73) Symons, M. R.; Zimmerman, D. N. *J. Chem. Soc., Dalton Trans.* **1975**, 2545.
(74) Huffadine, A. S.; Peake, B. M.; Robinson, B. H.; Simpson, J.; Dawson, P. A. *J. Organomet. Chem.* **1976**, *121*, 391.
(75) Lindsell, W. E.; Preston, P. N. *J. Chem. Soc., Dalton Trans.* **1979**, 1105.
(76) Fieldhouse, S. A.; Fullam, B. W.; Neilson, G. W.; Symons, M. R. *J. Chem. Soc., Dalton Trans.* **1974**, 567.
(77) Byers, B. H.; Brown, T. L. *J. Am. Chem. Soc.* **1977**, *99*, 2527.